Chapter 7
Unexpected Time Dependence in Nanofibrillated Cellulose Gels

Samir Patel and Jacob Notbohm

Abstract Nanofibrillated cellulose (NFC) gels behave similarly to a viscoelastic fluid, as the fibers create an entangled network interacting through van der Waals forces. NFC gels show complex mechanical behaviors, such as shear thinning and shear banding. Previous work has observed time-dependence on short time scales, observing relaxation times on the order of a few minutes, which is consistent with poroelastic behavior. Here, we report the surprising observation of time-dependent behavior over time scales of a few hours, implying that another mechanism dictates this behavior. NFC gels were thoroughly mixed with fluorescent particles for imaging on a spinning-disk confocal microscope. The gels were imaged for multiple hours, and the strains were computed using Fast Iterative Digital Image Correlation. Experiments first quantified strains in gels subjected to compression and in unloaded gels with various aspect ratios. The gels deformed for a few hours in the loading device regardless of whether a load was applied, and gels with high aspect ratios deformed over a few hours to become more circular. These results suggest that NFC gels may exhibit capillary behavior, which could be the mechanism for time dependence at long time scales. Further experiments quantified displacements in NFC gels when water was introduced by contracting microspheres to gather insight on poroelastic behavior. The gels moved inward towards the expelled water at short time scales, even though they were not adhered to the contracting microspheres. This work motivates future work to study in detail the effects of water on the mechanics of NFC gels over a wide range of time scales.

Keywords Hydrogels · Cellulose · Poroelasticity · Capillary · Time-dependence

Introduction

Nanofibrillated cellulose (NFC) gels are biodegradable and renewable, making them appealing for many uses, including 3D printing, food packaging, and drilling fluid [1]. Cellulose gels behave similarly to a viscoelastic fluid, as the fibers create an entangled network with van der Waals interactions. The different production methods used to create NFC can change the rheology and mechanics of the system by altering fiber geometry and cross-linking [2, 3]. NFC suspensions show complex fluid-like behaviors, such as shear thinning in a rheometer [1, 4]. Quantifying the rheology of NFC gels using commercial rheometers is challenging, because the measured modulus depends on sample thickness [5]. This is likely due to shear banding and strain localization near the boundaries of the sample, which cause inconsistencies in measured data of the rheological properties such as viscosity and shear modulus [6, 7]. These complications make the rheology of NFC gels challenging to quantify.

Cellulose gels are hydrophilic and swell substantially in the presence of water. Swelling behavior has been studied at larger length scales in cellulose sponges [8, 9] with results showing that the sponges swell with water on time scales of a few minutes. Previous work has measured time-dependent behavior in cellulose gels to be on the order of minutes in stress relaxation experiments [10]. Prior work has also suggested that cellulose gels exhibit poroelasticity, with a compressive relaxation time of around 16-160 s for cellulose gels of diameter on the order of centimeters [11]. Poroelasticity is common in other materials as well, including biological tissues [12], the cytoplasm within cells [13], and tendons [14]. The time scale of tens to hundreds of seconds for relaxation of centimeter-sized samples is also common. For example,

Samir Patel · Jacob Notbohm
Department of Mechanical Engineering
e-mail: spatel222@wisc.edu; jacob.notbohm@wisc.edu

Samir Patel · Jacob Notbohm
Engineering Mechanics Program, University of Wisconsin-Madison, 1500 Engineering Dr, Madison, WI 53706
e-mail: spatel222@wisc.edu; jacob.notbohm@wisc.edu

Karen Kasza et al. (eds.), *Mechanics of Biological Systems and Materials and the Mechanics of Composite, Hybrid & Multifunctional Materials, Vol. 3*, Conference Proceedings of the Society for Experimental Mechanics Series, https://doi.org/10.13052/97887-438-0829-9_7

polyvinyl alcohol-polyacrylic acid hydrogels of size on the order of centimeters have a stress relaxation time on the order of minutes [15].

In this report, we experimentally quantify the time-dependent properties of cellulose gels, observing surprising time dependence occurring at time scales on the order of hours. Three experiments were conducted to study the mechanics of the NFC gels. (i) Strains were quantified after NFC gels were subjected to compression. The mean strains over time showed a time dependence on the order of hours, which led to further experiments to explain this phenomenon. It was found that this long time dependence was due to interactions between the NFC gel and boundaries, suggesting possible capillary effects. (ii) The deformation of gels of various aspect ratios was discerned by quantifying strains when placed on hydrophilic substrates for a few hours, with results showing the gels deformed to become circular, suggesting a strong effect of surface tension. (iii) To study NFC gels' interaction with water at length scales close to the size of fibers, water was introduced to the cellulose gels by embedding poly(N-isopropylacylamide) (PNIPAAm) microspheres, which contract when heated [16, 17, 18]. Upon contraction, the microspheres left a void space filled with water, which the NFC gels expanded into over time scales of tens of minutes.

Methods

Tempo-Oxidized Nanofibrillated Cellulose (T-NFC) was provided by the Forest Products Laboratory (Madison, WI) as a 1.11 weight percent concentration. The NFC gels were vortex mixed with Alexa Fluor carboxylated fluorescent particles of 0.5 μm diameter and excitation and emission wavelengths of 580 and 605 nm, respectively (F8812, Thermo Fisher Scientific). The concentration of fluorescent particles in the NFC gels was chosen to be around 3.6 mg per 1 mL NFC. We compared pipette mixing and vortex mixing. Vortex mixing the fluorescent particles and NFC gel provided a more consistent mixture of fluorescent particles in the gel. Gels embedded with fluorescent particles were used in all experiments.

PNIPAAm microspheres were created through an adapted version of the methods from ref. [18]. The microspheres were created using an oil-water emulsion. Cyclohexane, span-80 (S0060, TCI America), N-isopropylacrylamide (415324, Millipore Sigma), bis-acrylamide (1610142, Bio-Rad), ammonium persulfate (1610700, Bio-Rad), and tris-buffered saline were mixed on a stir plate in a nitrogen atmosphere. TEMED was added during the mixing and the reaction occurred overnight. The microspheres were then washed with ethanol, deionized water, and 1× phosphate buffered saline.

In all experiments, NFC gels embedded with fluorescent particles were imaged on a spinning-disk confocal microscope (Yokogawa CSU-X1) with 50 μm pinholes, a 20× 0.95 NA water-immersion objective (Nikon), and a Zyla sCMOS camera (Andor). Image specifications were set through IQ3 acquisition software (Andor). All images were collected with a 150 ms exposure time. All z-stacks had a step size of 0.325 μm. The number of z-steps collected varied from about 50 (for experiments applying uniform strain) to about 150 (for experiments with PNIPAAm microspheres). When imaging NFC gels without PNIPAAm microspheres, the z-planes chosen for imaging were at least 60 μm above the glass substrate to avoid significant surface effects. When imaging gels with PNIPAAm microspheres, we chose planes at or close to the microspheres' centers. In both experiments, we experienced some drifting in all directions, which we manually accounted for during image acquisition. After acquiring the images, the z-stacks from different time points were registered to each other, enabling selection of the same focal plane at all time points for subsequent analysis by digital image correlation (DIC).

A custom-built loading device was used to apply compression to the NFC gels. The applied strain was actuated by a micrometer. The device was designed to fit in the microscope stage, so that images of the gels before and after applying strain could be taken. Strains were quantified in NFC gels when subjected to compression over a few hours. Strains were also quantified in unloaded gels placed either inside or outside of the loading device. To further test capillary behavior, NFC gels embedded with fluorescent particles were pipetted onto glass slides such that they either had a higher length (0.75 in) than their width (0.25 in) or were circular (radius 0.25 in). We imaged these gels every 5 min for up to 3 hr for subsequent analysis by DIC. To gain insight on poroelastic behavior, we carefully pipette-mixed PNIPAAm microspheres into NFC gels embedded with fluorescent particles, so the microspheres would not be damaged before the experiment. The microspheres acted as void inclusions in the gel, which decreased in volume when the temperature was raised from the reference temperature (29°C) to 39°C [17]. The temperature was controlled using an H301 stage top incubator (Okolab). This was mounted directly on the microscope stage so that imaging and changing the temperature of the environment could be performed simultaneously. During contraction, the PNIPAAm microspheres became hydrophobic and expelled water. We imaged the gel before and after the contraction of the microspheres, which typically occurred within 20-30 min. Microspheres selected for imaging were at least a field of view away from other microspheres to avoid effects from other microspheres.

DIC was used to quantify the displacements and strains, enabling us to avoid errors caused by strain localization. Fast Iterative DIC [19] was performed on all image sets to quantify the in-plane displacement fields. We used a subset size of

64 × 64 pixels (20.8 × 20.8 μm^2) and a spacing of 16 pixels (5.2 μm). DIC was performed by comparing each image to the corresponding image in the reference (undeformed) configuration. The strains were calculated from the gradient of displacements. Numerical derivatives were taken by finding slopes in the x and y directions in a kernel of a 5×5 window of points, which generates the displacement gradient at the center of the window [20]. This process was repeated throughout the entire image to compute the strain fields.

Results

We first quantified the DIC noise floor by quantifying strains from two consecutive images of an undeformed NFC gel embedded with fluorescent particles imaged with the confocal microscope (Fig. 1a). From the images, in-plane displacements were computed by DIC, and the in-plane components of the strain tensor were computed from the displacement field. The strain fields and histograms of ε_{xx}, ε_{yy}, and ε_{xy} did not exceed 0.5% (Fig. 1b,c). The histograms show that the noise was random and resembled a Gaussian distribution. The standard deviation of noise from this analysis was approximately 0.1% strain.

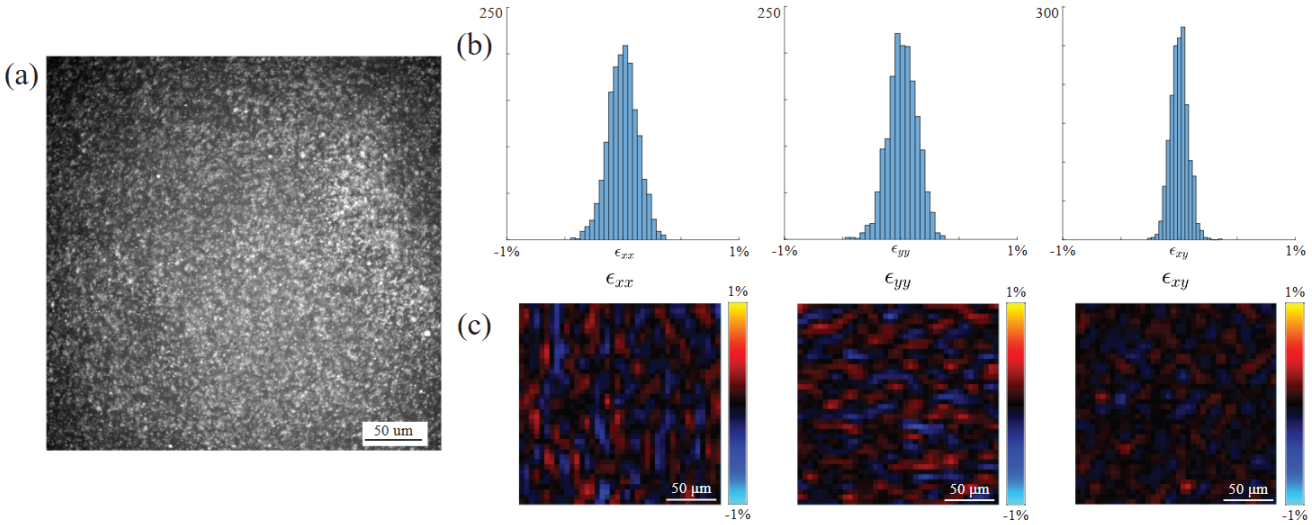

Fig. 1 Noise floor analysis on an NFC gel embedded with fluorescent particles. (a) Representative confocal image of NFC gel embedded with fluorescent particles. (b) Histograms of strains. (c) Strain fields. Results from panels b and c show that the noise in measured strains was less than 0.5%.

Next, we applied compression to NFC gels, as shown in Fig. 2a, using a custom loading device that was mounted on the microscope stage. Images were collected in a region of interest near the center of each gel, followed by calculation of displacements and strains by DIC. When the gels were compressed in the x direction, there was an immediate response in the strain in the region of interest, showing $\varepsilon_{xx} < 0$ which is expected for compression. The variability in strain over space, as indicated by the standard deviation, was relatively small, being approximately 1%, indicating that NFC gels are relatively homogeneous, even at scales of tens of microns, which differs from other fibrous materials such as gels of collagen [17, 18, 21]. Interestingly, ε_{xx} changed over time, increasing over a period of a few hours, which is unexpected given that the loading device applied a constant displacement at the boundaries of the sample. For the strains in the region of interest to change over time, the gel must have undergone a complex time-dependent deformation with increasing strain in the region of interest balanced by decreasing strain in other locations. The time dependence was also surprising, as it occurred on time scales of hours. Prior work on compressive relaxation on cellulose gels computed a relaxation time of around 16-160 s for samples that were centimeters in size [11]. In the theory of poroelasticity, the poroelastic time scale τ is related to sample size L such that the expression τ/L^2 is constant [22]. Using this expression and the prior data τ = 160 s and L = 2 cm, we would expect our samples having size of ≈ 2.5 cm would have a characteristic poroelastic time of around 4 min, which is far shorter than the time scales for deformation shown in Fig. 2a. Hence, there must be some other mechanism that drives the deformation of these gels.

NFC gels were next placed in the loading device but not subjected to compression, with the expectation that the gel would remain undeformed. Surprisingly, ε_{xx} increased over a time period of a couple of hours (Fig. 2b). This may suggest that the deformation was caused by interaction between the sample and the loading device. To verify this, we placed gels on a glass coverslip outside of the loading device. When quantifying strains with DIC, ε_{xx} was near zero for all time points (Fig. 2c). This indicates that the sample interacted with the loading device, causing time-dependent deformation. We reasoned that the interaction could be through differences in surface tension of the NFC gel in the different conditions. This suggests that NFC gels may exhibit elasto- or visco-capillary behavior.

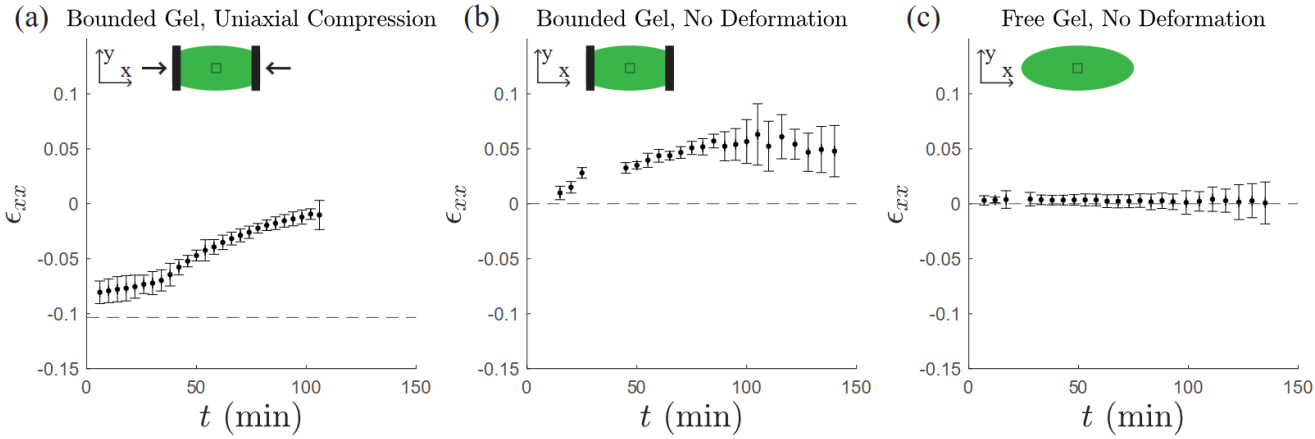

Fig. 2 Strains in experiments with NFC gels. (a) NFC gels were placed in the loading device and were subjected to uniaxial compression in the x direction. Time $t = 0$ denotes when the deformation was applied. (b) NFC gels were placed in the loading device but not subjected to any loading. ε_{xx} shows that despite no loading, the strain increased over a period of a couple of hours. (c) NFC gels were not placed in the loading device. The strains in these gels were near zero for the duration of the experiment. All images show cartoons of NFC gels (green) and the location imaged by the microscope (squares). Panels a and b show the gel in the loading device (black). In all images, ε_{xx} is quantified through DIC and averaged at each time point. Dots in each image denote the mean strain, and error bars denote standard deviations over space. The dashed line denotes the macroscale strain applied by the loading device on the gel.

As a simple initial quantification of capillary behavior, we placed NFC gels of various aspect ratios on glass coverslips and imaged them for a few hours. Some gels had length-to-width ratios of 3:1, while other gels were circular. The average strains are shown in Fig. 3. For the elongated gels, the normal strains along the short axis (y direction) increased over an hour (Fig. 3b). This indicates that the gels deformed to become more circular. Deformations of the gels were apparently permanent, as the gels did not return to their initial size and shape. By contrast, the circular gels remained essentially undeformed with strains being approximately zero for all time points (Fig. 3c). Because we did not apply a load on the gels during these experiments and elongated gels became circular, the gels' deformation was likely caused by surface tension, consistent with capillary behavior.

We next quantified the response of NFC gels to introduction of a void space containing water. This experiment was intended to give a sense of poroelastic swelling at a length scale close to that of the fibers, which is a smaller length scale than the experiments in Figs. 2–3. To create void space in the NFC gels, we used microspheres of PNIPAAm, a hydrogel that contracts and expels water when heated. Microspheres were added to NFC gels embedded with fluorescent particles. An image was collected at 29°C followed by increasing the temperature to 39°C, which caused the microspheres to contract and expel water. A second image was collected for subsequent quantification of displacements by DIC. Fig. 4a shows a schematic of the described experiment, wherein a PNIPAAm microsphere (black) contracts and pushes water out, indicated by the white region. For most engineering materials, this experiment would cause no deformations, because the PNIPAAm microspheres were not attached to the surrounding material, but the NFC gel could potentially swell in response to the free water. Fig. 4b displays a representative image in the reference state, with the PNIPAAm microsphere being the black circle in the center of the image and the contrast provided by the fluorescent particles embedded in the NFC gel. After contraction, the fluorescent particles appeared to move inward (Fig. 4c), indicating inward deformation of the NFC gel. The inward deformation was confirmed in the displacements quantified by DIC, with a maximum magnitude of displacement of ≈5 μm (Fig. 4d). This inward motion was likely due to swelling of the NFC into the region containing water expelled by the contracting microsphere.

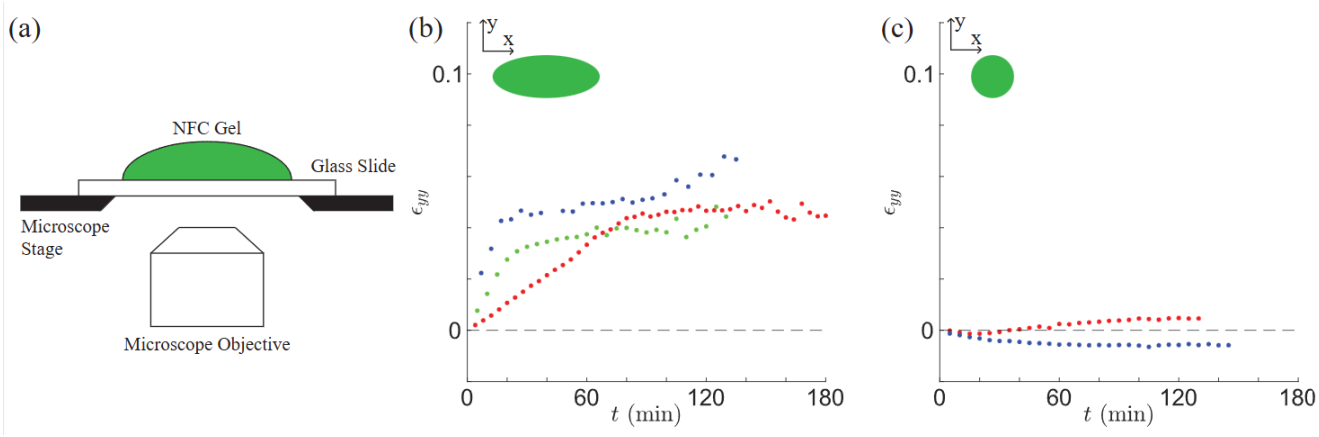

Fig. 3 Mean strains in free NFC gels of two different aspect ratios. (a) Imaging setup for quantifying strains in elongated or circular gels. (b) Elongated gels, where the length of the gel (≈0.75 in) was much larger than its width (≈0.25 in). Here, ε_{yy} increased over time, indicating elongation of short axis so the gel became more circular. (c) Circular gels, with radii close to the width of the long gels. Here, $\varepsilon_{yy} \approx 0$ for all time points. In subfigures (b-c), colors denote results from different samples. In all experiments between both shapes, ε_{xx} was approximately zero for all time points.

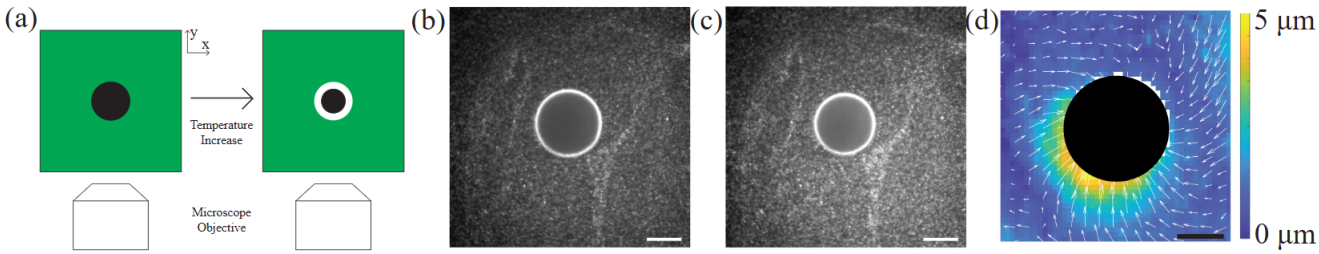

Fig. 4 Local displacements in an NFC gel. (a) Schematic of contracting PNIPAAm microspheres in NFC gel. The microspheres are not physically or chemically adhered to the NFC. The white space around the contracted microsphere denotes water that NFC can expand into. (b-c) Images of NFC gel before (b, 29°C) and after (c, 39°C) contraction of a representative PNIPAAm microsphere. (d) Local displacements quantified through DIC. The color indicates magnitude of displacements, and arrows show direction and magnitude. White regions in the displacement field are erroneous regions that are removed from the analysis as in ref. [17]. The black circle indicates the location of the microsphere; it is larger than the size of the microsphere, as DIC can not get proper data at boundaries in the image. All scale bars denote 50 μm.

Conclusions

In this report we have shown an unexpected time dependence, with deformations occurring on the order of hours in gels made of NFC. Subsequent investigation showed that elongated gels on hydrophilic substrates deformed to become more circular, suggesting capillary behavior may be the underlying cause for the long time dependence. The experiments with PNIPAAm microspheres revealed that NFC gels swelled into the water expelled by the PNIPAAm. These observations, combined with prior studies on poroelastic effects in NFC gels, indicate that the mechanics of NFC gels results from a combination of swelling, poroelasticity, and capillary behavior.

Future work will design experiments to test this combination of properties in more detail. A challenge to consider in future work is drying of the gels, which occurs on time scales of hours, similar to the time scales of deformation observed in this study. In the experiments shown in Fig. 2, it would not be possible to wait for the sample to equilibrate in the loading device before testing, because the hours of equilibration time would cause the sample to dry excessively. Experiments are being designed to use samples having dimensions that minimize the surface area exposed to air, which will enable rigorous quantification of mechanical properties.

Acknowledgments We thank John Considine and the Forest Products Laboratory for providing the NFC used in this study. This work was supported by the Department of Mechanical Engineering at UW-Madison and by the United States Endowment for Forestry and Communities grant number 22-CA-11111129-049. The United States Endowment for Forestry and Communities, Inc. is a not-for-profit corporation that collaborates with partners in the public and private sectors to advance systemic, transformative, and sustainable change for the health and vitality of the nation's working forests and forest-reliant communities.

References

1. M.-C. Li, Q. Wu, R. J. Moon, M. A. Hubbe and M. J. Bortner, "Rheological Aspects of Cellulose Nanomaterials: Governing Factors and Emerging Applications," Advanced Materials, vol. 33, p. 2006052, 2021. W409W10080
2. K. Missoum, M. N. Belgacem and J. Bras, "Nanofibrillated Cellulose Surface Modification: a Review," Materials, vol. 6, p. 1745–1766, 2013. W409W10080
3. H. A. Khalil, Y. Davoudpour, M. N. Islam, A. Mustapha, K. Sudesh, R. Dungani and M. Jawaid, "Production and Modification of Nanofibrillated Cellulose Using Various Mechanical Processes: a Review," Carbohydrate Polymers, vol. 99, p. 649–665, 2014. W409W10080
4. S. Mohan, G. H. Koenderink and K. P. Velikov, "Inelastic Behaviour of Cellulose Microfibril Networks," Soft Matter, vol. 14, p. 6828–6834, 2018. W409W10080
5. A. Pakzad, "Size Effects on the Nanomechanical Properties of Cellulose I Nanocrystals," Journal of Materials Research, vol. 27, pp. 528-536, 2011. W409W10080
6. O. Nechyporchuk, M. N. Belgacem and F. Pignon, "Current Progress in Rheology of Cellulose Nanofibril Suspensions," Biomacromolecules, vol. 17, p. 2311–2320, 2016. W409W10080
7. O. Nechyporchuk, M. N. Belgacem and F. Pignon, "Rheological Properties of Micro-/Nanofibrillated Cellulose Suspensions: Wall-Slip and Shear Banding Phenomena," Carbohydrate Polymers, vol. 112, p. 432–439, 2014. W409W10080
8. J. Ha, J. Kim, Y. Jung, G. Yun, D.-N. Kim and H.-Y. Kim, "Poro-Elasto-Capillary Wicking of Cellulose Sponges," Science Advances, vol. 4, p. eaao7051, 2018. W409W10080
9. J. Kim, J. Ha and H.-Y. Kim, "Capillary Rise of Non-Aqueous Liquids in Cellulose Sponges," Journal of Fluid Mechanics, vol. 818, p. R2, 2017. W409W10080
10. P. Lopez-Sanchez, M. Rincon, D. Wang, S. Brulhart, J. R. Stokes and M. J. Gidley, "Micromechanics and Poroelasticity of Hydrated Cellulose Networks," Biomacromolecules, vol. 15, p. 2274–2284, 2014. W409W10080
11. M. R. Bonilla, P. Lopez-Sanchez, M. J. Gidley and J. R. Stokes, "Micromechanical Model of Biphasic Biomaterials With Internal Adhesion: Application to Nanocellulose Hydrogel Composites," Acta Biomaterialia, vol. 29, p. 149–160, 2016. W409W10080
12. E. E. Konofagou, T. P. Harrigan, J. Ophir and T. A. Krouskop, "Poroelastography: Imaging the Poroelastic Properties of Tissues," Ultrasound in Medicine & Biology, vol. 27, p. 1387–1397, 2001. W409W10080
13. E. Moeendarbary, L. Valon, M. Fritzsche, A. R. Harris, D. A. Moulding, A. J. Thrasher, E. Stride, L. Mahadevan and G. T. Charras, "The Cytoplasm of Living Cells Behaves as a Poroelastic Material," Nature Materials, vol. 12, p. 253–261, 2013. W409W10080
14. B. K. Connizzo and A. J. Grodzinsky, "Tendon Exhibits Complex Poroelastic Behavior at the Nanoscale as Revealed by High-Frequency AFM-Based Rheology," Journal of Biomechanics, vol. 54, p. 11–18, 2017. W409W10080
15. P. Chiarelli, D. De Rossi and P. Basser, "Hydrogel Stress-Relaxation," Journal of Intelligent Material Systems and Structures, vol. 4, p. 176–183, 1993. W409W10080
16. M. Proestaki, A. Ogren, B. Burkel and J. Notbohm, "Modulus of Fibrous Collagen at the Length Scale of a Cell," Experimental Mechanics, vol. 59, p. 1323–1334, 2019. W409W10080
17. B. Burkel and J. Notbohm, "Mechanical Response of Collagen Networks to Nonuniform Microscale Loads," Soft Matter, vol. 13, p. 5749–5758, 2017. W409W10080
18. B. Burkel, M. Proestaki, S. Tyznik and J. Notbohm, "Heterogeneity and Nonaffinity of Cell-Induced Matrix Displacements," Physical Review E, vol. 98, p. 052410, 2018. W409W10080
19. E. Bar-Kochba, J. Toyjanova, E. Andrews, K.-S. Kim and C. Franck, "A Fast Iterative Digital Volume Correlation Algorithm for Large Deformations," Experimental Mechanics, vol. 55, p. 261–274, 2015. W409W10080
20. H. Farid and E. P. Simoncelli, "Differentiation of Discrete Multidimensional Signals," IEEE Transactions on Image Processing, vol. 13, p. 496–508, 2004. W409W10080
21. M. Sarkar and J. Notbohm, "Quantification of Errors in Applying DIC to Fiber Networks Imaged by Confocal Microscopy," Experimental Mechanics, vol. 62, p. 1175–1189, 2022. W409W10080
22. A. H.-D. Cheng, Introduction, in "Poroelasticity," S. M. Hassanizadeh and J. Bear, Eds., Theory and Applications of Transport in Porous Media (pp. 1-59), Springer, 2016.W409W10080